SUPPORTING INFORMATION

Fullerene-based triplet spin labels: methodology aspects for pulsed dipolar EPR spectroscopy

Ivan O. Timofeev,[‡a] Larisa V. Politanskaya,[b] Evgeny V. Tretyakov,[c] Yuliya F. Polienko,[b] Victor M. Tormyshev,[b] Elena G. Bagryanskaya,[b], Olesya A. Krumkacheva*[a] and Matvey V. Fedin*[a]

[a] International Tomography Center SB RAS Novosibirsk, 630090, Russia.
[b] N.N.Vorozhtsov Institute of Organic Chemistry SB RAS Novosibirsk, 630090, Russia.
[c] N.D. Zelinsky Institute of Organic Chemistry RAS, Russia.

Table of content

1. Experimental equipment details

Exploited 150 W amplifier is the semiconductor-based know-how device elaborated by research institute NIIPP (https://www.niipp.ru) located in Tomsk, Russia. It is designed specifically for Q-band EPR sensitivity enhancement purposes. The amplifier is triggered by external blanking pulse, which comes from Bruker Elexsys E580 hardware and is adjusted via Bruker spectrometer software Xepr. Detection diode is protected by TTL microwave switch (Kratos Millimeter Wave SPST Switch Model F9014) with 70 dB isolation. All pulse EPR experiments were performed using the maximum available MW power, which is limited by a peak power of the protection switch. In order to limit the peak power, attenuation of 10 dB was accomplished using SMA-SMA microwave attenuators.

We employed a second harmonic (532 nm) of high-energy diode-pumped laser LOTIS TII LS-2146. Most of the experiments were done at 10 Hz repetition rate and diode current of 90-96 A, which gives 4-8 mJ pulse energy at the laser output and 2-6 mJ pulse energy at the terminus of optic fiber (50-70% lightguide conversion). The light path is sketched in Figure S1. The terminus of the optic fiber was positioned 1 cm above the solvent in a tube. Inserting the optic fiber directly into the tube provides a more efficient photoexcitation of all C_{60} molecules compared to illumination through the optical window of the resonator. This approach does not

involve the sealing of the end of the tube and, accordingly, controllable degassing of the sample. For this reason, no deoxygenation was performed and the influence of oxygen was not studied. The duration of the laser pulse (FWHM) was 15 ns with 150 ps std.dev., jitter was 500 ps, which is negligible on a nanosecond timescale of PD EPR experiments.

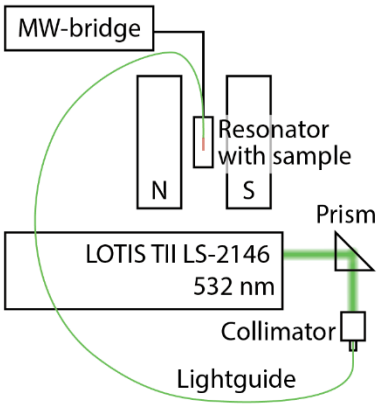

Figure S1. Sketch of the laser light path to a sample positioned in resonator.

2. Solvent glass cracking upon irradiation

In this work, we studied model dyads in toluene glass. Although the employed laser allows higher shot repetition rate, most of experiments were performed at 10 Hz pulsing due to the following reasons. Upon shock freezing toluene samples form either apparently perfect glass in the whole volume of the sample, or partially cracked glass consisting of eye-visible domains with ~1 mm characteristic size. Such medium is transparent and allows exciting all fullerenes in the sample. However, the quality of primarily obtained glass degrades over irradiation time, where glassy domains decrease in size and, as a result, overall transparency becomes poorer. Within several hours of irradiation the spectrum stops changing, presumably due to formation of a medium more stable to further irradiation (Figure S2). Upon thawing and refreezing glass is regenerated and the spectrum fully restores. Note, that fullerenes are known to have a negligible photobleaching at 532 nm in liquids [S2], in frozen solutions it should be even less efficient.

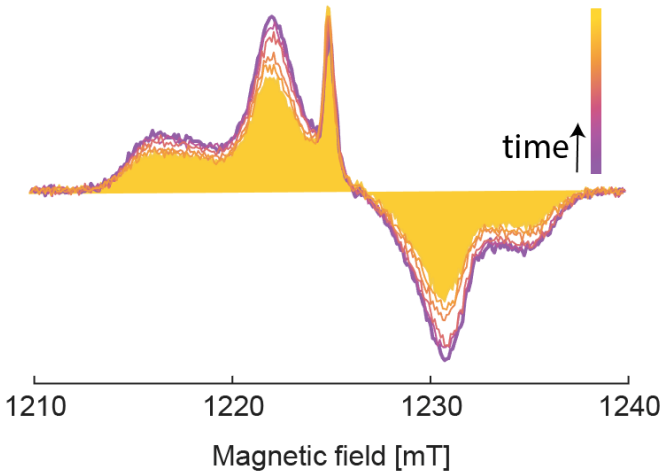

Figure S2. Q-band ED EPR spectrum of C_{60}TAM vs. irradiation time (1-3 hours in total). Filled spectrum is stable and does not degrade further on a scale of hours.

The described cracking of toluene glass is conditioned by heating due to a laser irradiation. Already at 10 Hz we observe averaged heating of the sample by 1-2 K, meaning that the peak heating on the nanosecond timescale might be even higher. This heating is inhomogeneous and generates defects/cracks in the glass. Moreover, it is power dependent, therefore 10 Hz was chosen to provide moderate mean power (<100 mW, <10 mJ/pulse) in order to avoid excessive opacity of the glass, prohibiting efficient excitation of fullerenes by light.

There is an additional reason not to raise the repetition rate above 10 Hz in experiments with observation on stable NIT/TAM radicals (RIDME and LaserIMD). The increase of the repetition rate, for instance, to 100 Hz would require an increase of temperatures to 50-80 K to provide conditions where longitudinal relaxation does not suppress observed echoes of stable radicals. The latter would decrease sensitivity and, in addition, ease the cracking of glassy medium.

Table S1. PD EPR experimental details. Common pulse sequence parameters: d_1 = 400 ns, d_2 = 1000 ns (see Figure 2 in manuscript for notation), Δt = 4 ns. Factor is accounted in mod. depths and SNRs as linear multiplication. The relative SNR number is the gain relative to SNR of NIT-NIT DEER (1000 Hz) at the corresponding band. Data at X-band is taken from ref. [S1].

Sample	Method	T, K	π_{obs} / π_{pump}, ns	Mod. depth, %	SNR	Relative SNR	Factor	Mod. depth (accounted factor), %	SNR (accounted factor)	Relative SNR (accounted factor)
C_{60}NIT (10 Hz)	Q-band LiDEER	20	20/16	21.2	14.9	0.24	1.05	21.2	15.6	0.25
	Q-band LiRIDME	20	20/-	25.8	6.1	0.10	1.05	27.1	6.4	0.10
	Q-band ReLIMD	20	20/-	16.1	19.7	0.31	1.18	19.0	23.3	0.37
	X-band LiDEER	20	20/24	34.0	36.2	1.9	-	-	-	1.9
C_{60}TAM (10 Hz)	Q-band LiDEER	30	16/18	65.5	107.8	1.7	1.30	65.5	140.1	2.2
	Q-band LiRIDME	30	20/-	22.4	37.8	0.60	1.30	29.1	49.1	0.78

	Q-band ReLIMD	30	20/-	23.3	30.9	0.49	1.05	24.5	32.4	0.51
	X-band LiDEER	20	24/28	82.0	89.7	4.7	-	-	-	4.7
NIT-NIT (1000 Hz)	Q-band DEER	50	20/18	30.0	63.2	-	-	-	-	-
	X-band DEER	50	28/22	37.0	19.2	-	-	-	-	-

The transparency loss is an indirect effect and does not reflect principal features of PD EPR methods. In order to provide consistent data and correctness of comparison, the modulation depth and SNR numbers took into account the cracking factor as follows. The experiment shown in Figure S2 features a 35% decrease of triplet C_{60} echo, when the 'quasi-stationary' condition is achieved, and this is typical. Being aware of this effect, we have monitored triplet C_{60} echo while recording PD EPR time traces and retrieved factors reflecting how damped SNR is in each particular experiment. These experimentally derived factors were applied to intensity in LiDEER and modulation depths in LiRIDME and LaserIMD (Table S1). Note that the main text of manuscript reports originally obtained values without correction for a cracking.

3. Spectra and relaxation properties

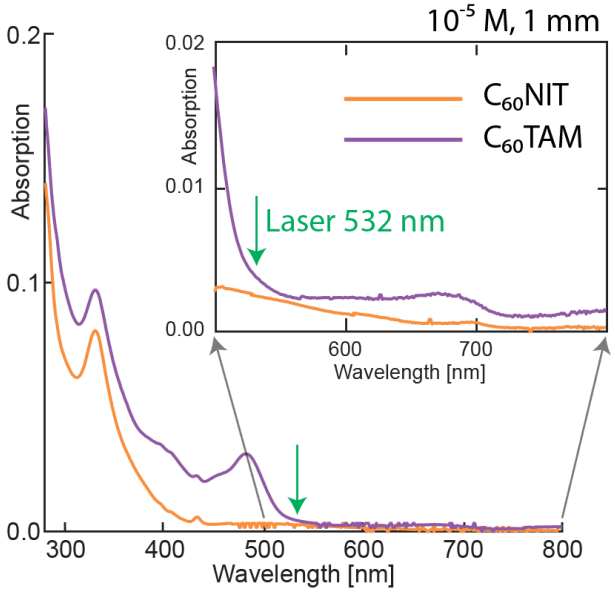

Figure S3. Optical spectra of studied dyads C_{60}NIT and C_{60}TAM. Dyads were dissolved in toluene at 10^{-5} M concentration. Spectra were recorded at room temperature with 1 mm optical path employing Agilent Cary 60 UV-Vis Spectrophotometer. Green arrow indicates the wavelength 532 nm used to generate triplet fullerenes in PD EPR experiments.

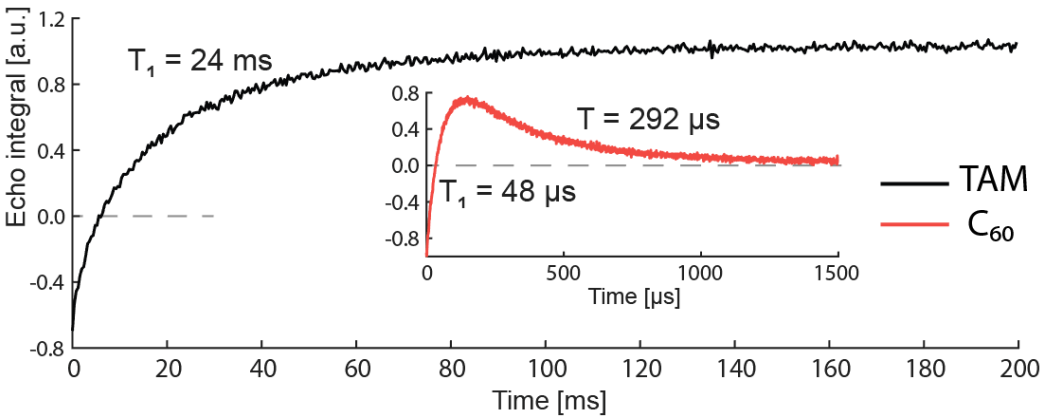

Figure S4. Inversion-recovery experiments on both components of C_{60}TAM dyad at 30 K. Exponential time constants are indicated on corresponding rises and decays. Triplet C_{60} features biexponential behavior, the fast recovery is considered as longitudinal relaxation with T_1 = 48 µs, while the slow decay time constant T = 292 µs describe triplet quenching. The time T = 292 µs correlates, but differs from $T_{triplet}$ = 360 µs, obtained in 2-pulse Hahn-echo experiment sweeping the delay between laser-pulse and MW-sequence (Figure 8 in manuscript), due to combination of triplet decay with relaxation processes in inversion-recovery experiment.

Triplet fullerene lifetime of 360 µs at the lowest temperatures suggest possible repetition rate up to 2500 Hz of a LiDEER experiment with triplet fullerene observer, so technically the lowest temperature is the optimum one providing the longest phase memory time. DEER experiment on NIT-NIT was optimized in the sense of T_1 vs. Boltzmann: temperature of 50 K allowed 1000 Hz repetition rate, which does not suppress nitroxide magnetization in toluene solution.

Table S2. Relaxation properties of triplet C_{60} and stable NIT and TAM radicals. Transverse relaxation times T_2 were measured in 2-pulse Hahn-echo experiment sweeping the delay between MW-pulses. Longitudinal relaxation times T_1 were measured in inversion-recovery experiment (Figure S4). Triplet lifetime $T_{triplet}$ was measured in 2-pulse Hahn-echo experiment sweeping the delay between laser-pulse and MW-sequence (Figure 8 in manuscript).

Dyad	component	T_2 (exponential time constant)	T_2 (stretched exp. time const / power)	T_1	$T_{triplet}$
C_{60}NIT (20 K)	triplet C_{60}	3.8 µs	4.4 µs / 1.4	51 µs	-
	nitroxide	3.5 µs	4.2 µs / 1.4	22 ms	-
C_{60}TAM (30 K)	triplet C_{60}	3.8 µs	4.3 µs / 1.3	48 µs	360 µs
	trityl	2.6 µs	3.1 µs / 1.6	24 ms	-

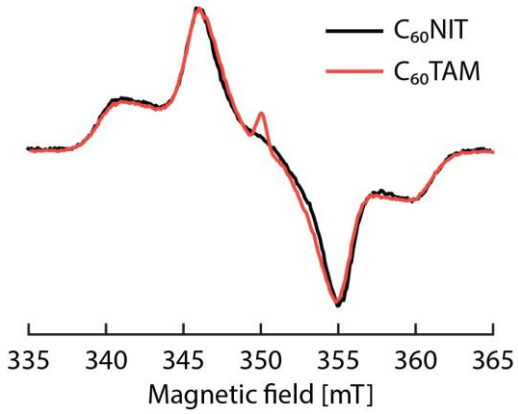

Figure S5. X-band ED EPR spectra (taken from ref. [1]) recorded at MW power optimal for triplet fullerene echo, which is 4 times stronger than the TAM one due to triplet hyperpolarization.

4. PD EPR data

4.1. DEER

The DEER acquisition parameters for 100 nM C_{60}TAM sample were set up using the identical (volume/size/solvent) sample with 2 μM concentration; this was done to ease observation of an echo and all adjustments with a reasonable number of repetitions. After the setup, the 100 nM sample was placed into resonator, and DEER trace was accumulated during 42 hours. Only a signal phase was adjusted during this accumulation. Usually automatic (implemented in PulseSpell program) phase cycling of the first $\pi/2$ pulse is applied in order to eliminate constant SpecJet offset. However, for the sake of stability we ran experiment from Xepr tables and cycled the first pulse manually (by collecting a certain number of scans with one or another phase during a few hours and then summing them). The stability here implies continuous laser shooting (evenly spaced laser pulses) and quasi-stable power, which is possible only for experiments run from Xepr tables. The signal phase was adjusted after signal became visible, which occurred in a few hours; as a result, an unequal number of differently phased DEER traces were acquired with acceptable phase. This eventually led to the loss of information about modulation depth, but not more, since unsubtracted SpecJet offset is constant.

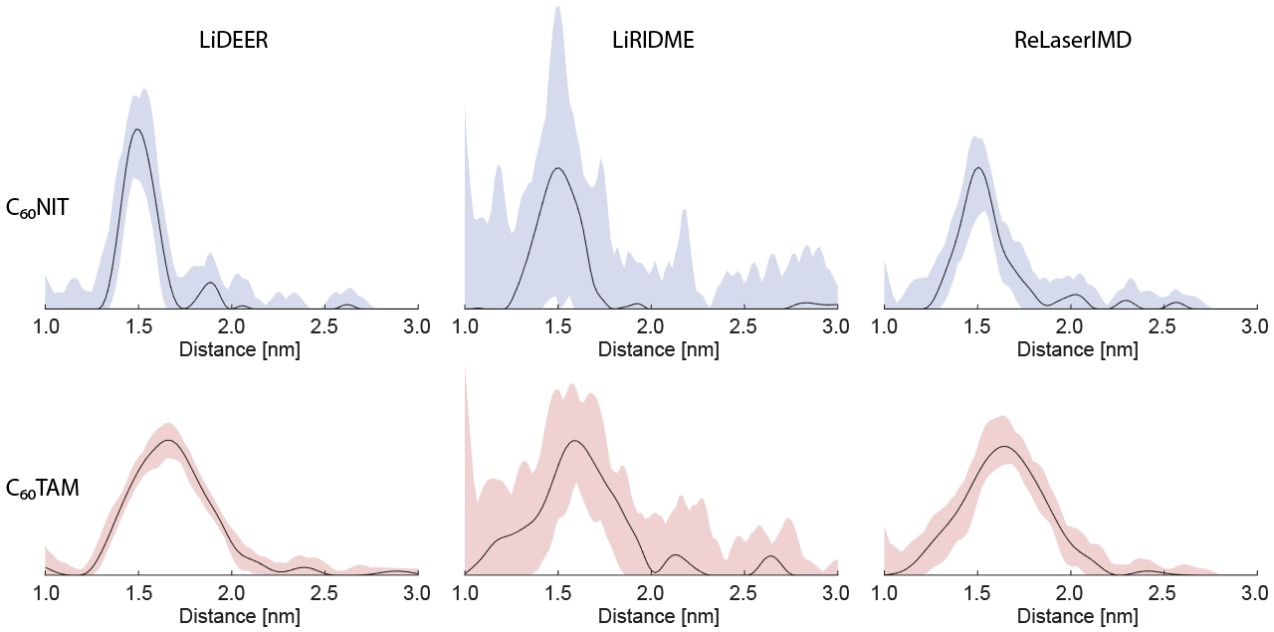

Figure S6. Distance distributions (black lines) with uncertainty margins (blue patch – C_{60}NIT, red patch – C_{60}TAM) calculated via Monte Carlo validation by doubling the noise level (DeerAnalysis2019 validation tool). LiRIDME signals involve the burst of noise at the last part of time traces, so doubling of it leads in some cases to a significant drop of modulation depth and consequent reduction of distribution integral.

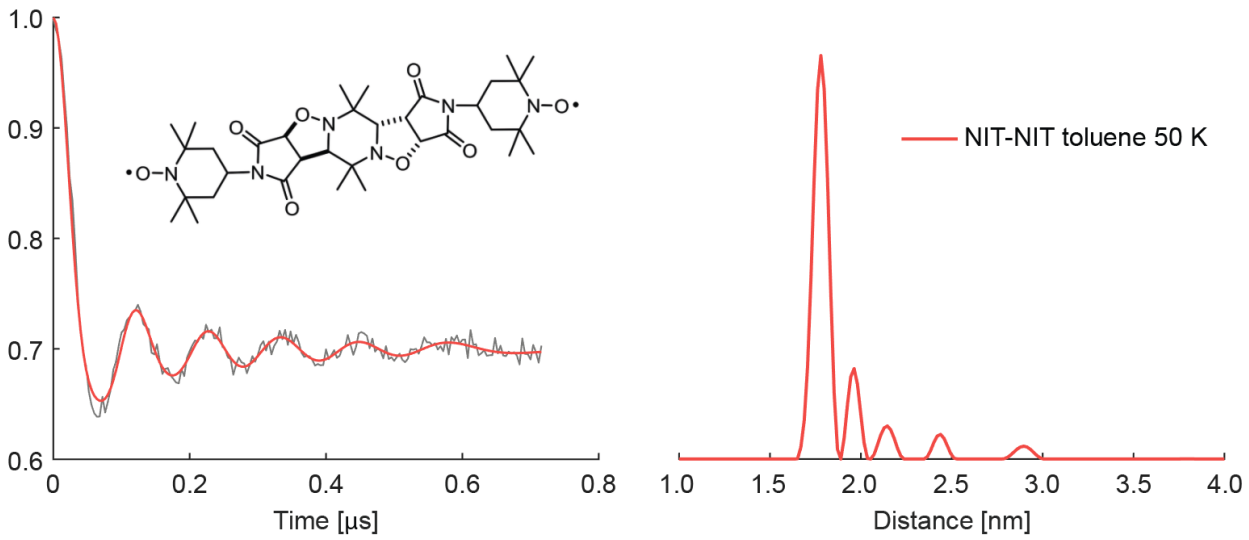

Figure S7. Q-band DEER time trace and distance distribution of model NIT-NIT. Chemical structure is shown above the time trace. NIT-NIT biradical used as reference for sensitivity characterization was dissolved in toluene in 10^{-5} M concentration and 10 µL volume.

4.2. RIDME

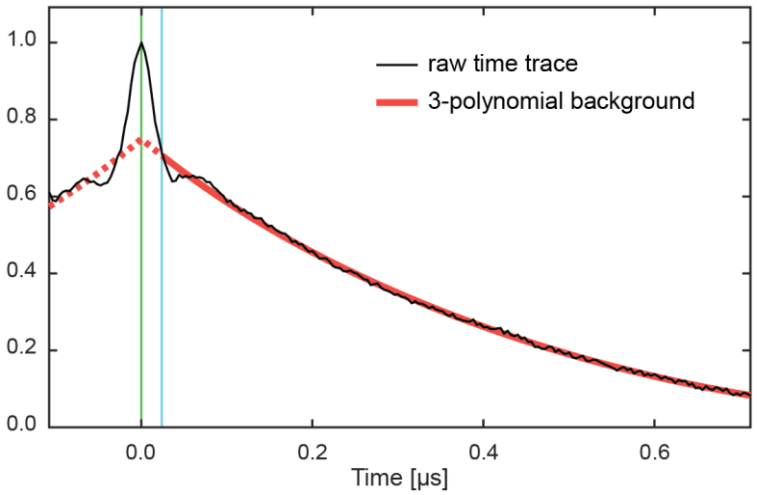

Figure S8. C_{60}NIT LiRIDME raw time trace with 3-polynomial background function applied phenomenologically. As the function is quite steep, background correction leads to the burst of noise at the last part of the trace.

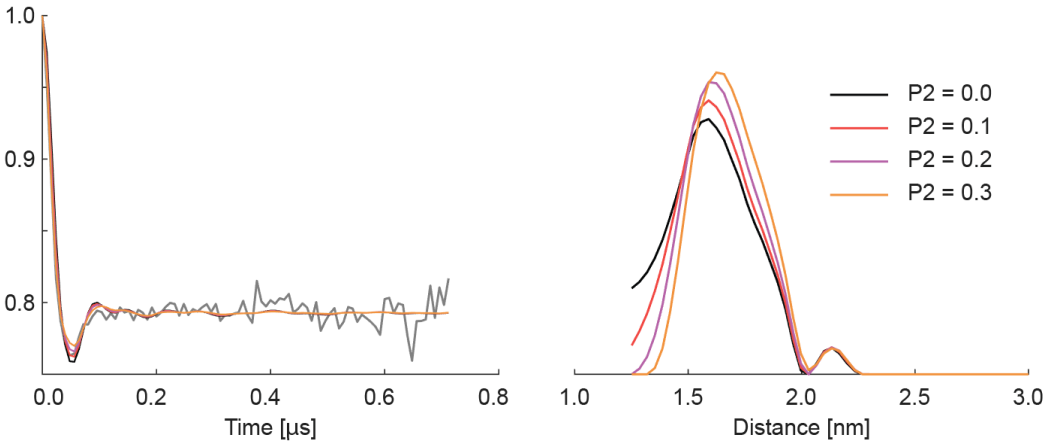

Figure S9. C_{60}TAM LiRIDME time trace along with fits (left) and distance distributions (right) obtained using OvertoneAnalysis[S3] with second harmonic overtone P2, whose ratio is indicated in the legend. Given overtones fit the modulations acceptably, but resulting distance distributions cannot be strictly validated, as the distances are extremely small and other PD EPR methods have restraints; DEER does not resolve short distances and ReLaserIMD has the artifact.

4.3. LaserIMD

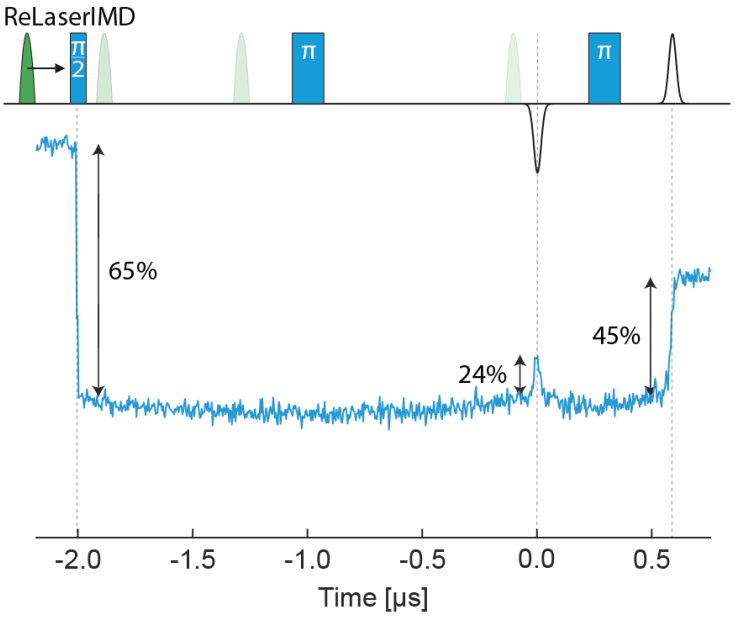

Figure S10. Extended ReLaserIMD time trace of C_{60}NIT. The first intensity drop is the direct LaserIMD evolution that features 65% modulation depth; major part of this drop is conditioned by the disappearance of triplet C_{60} signal at observer position. The intermediate signal with 24% modulation depth is considered to be the undistorted ReLaserIMD dipolar signal (mod. depth differs from 19% designated in Table S1 due to the glass cracking). The last one is the reverse LaserIMD evolution signal with 45% modulation depth artificially increased due to the disappearance of the observer signal in folded dyads.

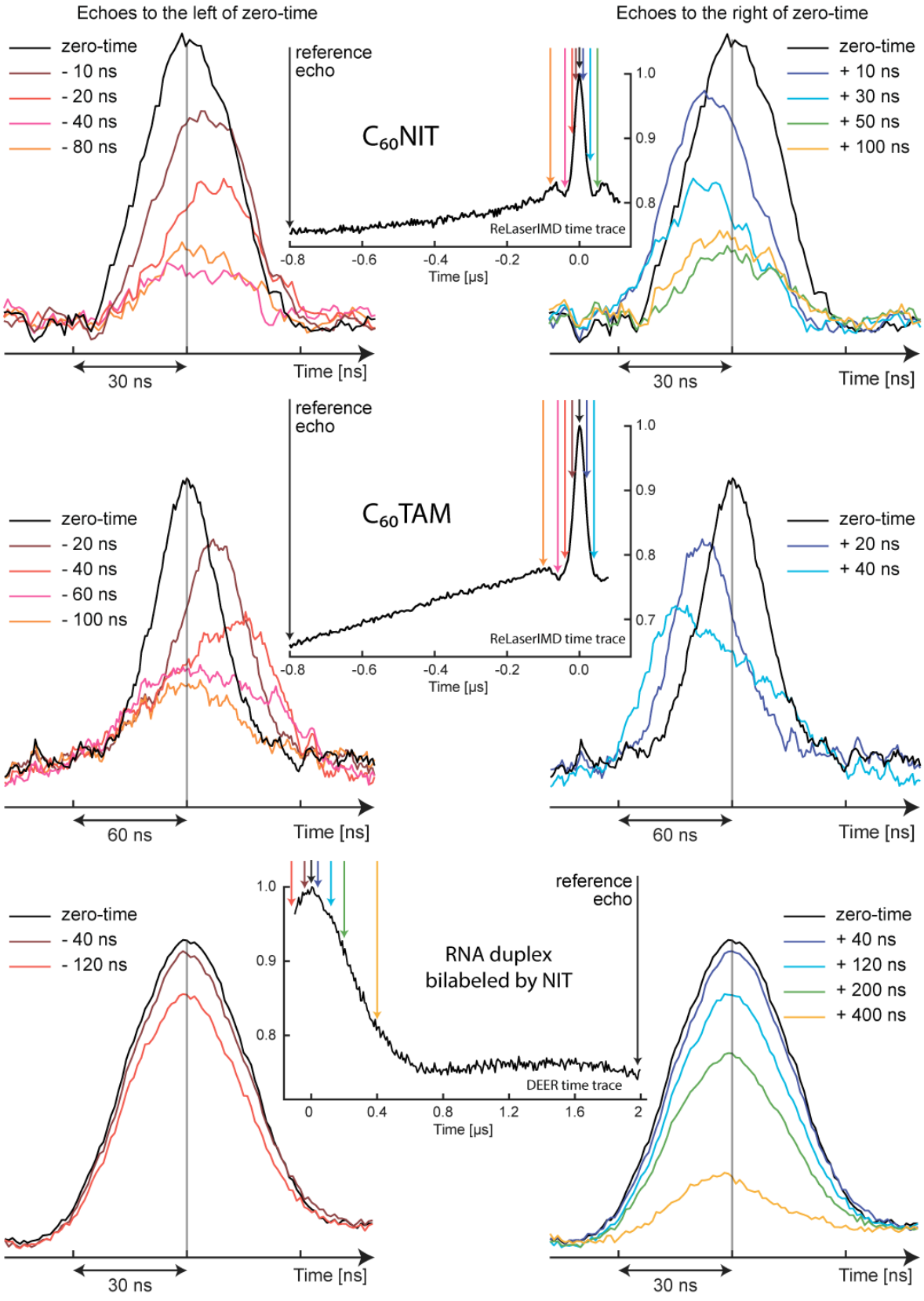

Figure S11. ReLaserIMD experiment. (Top, middle) For clarity the alternating shapes of the observed echoes are presented with the reference echo subtracted. Reference echo is detected at 800 ns to the left relative to zero time, the position of reference is designated in time traces. (Bottom) Persistent shapes of observed echo in DEER performed on RNA duplex labeled by two nitroxides (experimental setup: Q-band, 50 K, 10 µL of D_2O-glycerol-d_8 solvent, π_{obs}=24 ns, π_{pump}=22 ns). These data are provided for comparison.

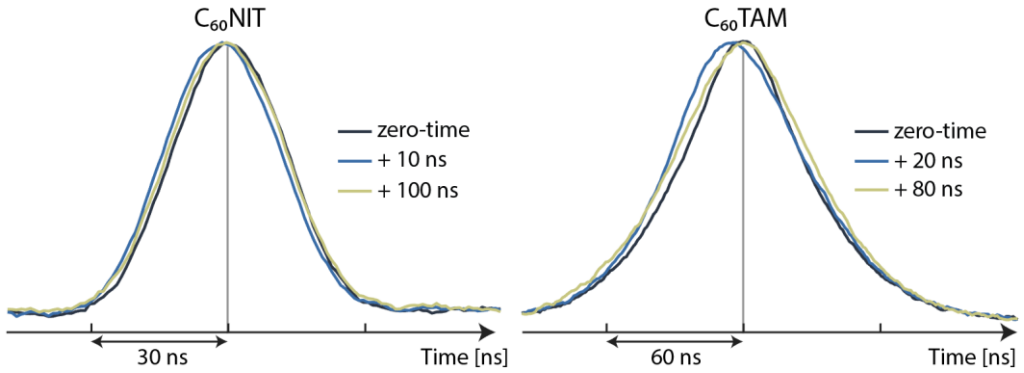

Figure S12. Normalized ReLaserIMD observed echoes to the right of zero time. Blue colored echoes are the ones with the most shifted centers. Olive colored echoes do not change in shape upon further evolution and feature the same shape as NIT/TAM echoes without photoexcitation.

4.4. Signal to Noise Ratios

The smoothing spline parameter for SNR estimation ($2 \cdot 10^{-3}$ on the nanosecond timescale, same as in ref. [S1]) has been chosen on the basis of two criteria: the dipolar modulation is not oversmoothed, and (ii) the noise is not overfitted. Although this method filters out low frequencies including dipolar ones, it is consistent among all traces where it is applied. SNR numbers obtained using Tikhonov regularization suffer from both imperfect background elimination and imperfect fitting of dipolar modulations, which alter from trace to trace. This is especially evident in the case of reference DEER experiment on NIT-NIT sample even with low regularization parameter (Figure S7 and Table S3). The relative SNR gain is of primary interest; therefore, in our opinion, the uniformity in mathematical calculation of SNR for all traces is more important than following physical reasoning at the expense of consistency.

Table S3. Different estimates of SNR numbers for Q-band PD EPR experiments. SNR_1 is calculated as the inverse RMSE of a smoothing spline fit of a real part normalized on modulation depth (Figure 9). SNR_2 is calculated as inverse RMSE of the same spline fit of an imaginary part multiplied by modulation depth. SNR_3 is calculated as inverse RMSE of Tikhonov regularization fit multiplied by modulation depth.

Sample	Method	SNR_1	SNR_2	SNR_3
C_{60}NIT (10 Hz)	LiDEER	14.9	10.3	13.1
	LiRIDME	6.1	25.1	5.1
	ReLaserIMD	19.7	19.6	16.1
C_{60}TAM (10 Hz)	LiDEER	107.8	100.3	87.0
	LiRIDME	37.8	96.9	30.9
	ReLaserIMD	30.9	35.1	29.3
NIT-NIT (1000 Hz)	DEER	63.2	61.4	44.0

5. References

[S1] O. A. Krumkacheva, I. O. Timofeev, L. V. Politanskaya, Y. F. Polienko, E. V. Tretyakov, O. Y. Rogozhnikova, D. V. Trukhin, V. M. Tormyshev, A. S. Chubarov, E. G. Bagryanskaya and M. V. Fedin, Triplet Fullerenes as Prospective Spin Labels for Nanoscale Distance Measurements by Pulsed Dipolar EPR Spectroscopy, Angew. Chem. Int. Ed. 2019, 58, 13271–13275.

[S2] A. A. Krasnovsky and C. S. Foote, Time-resolved measurements of singlet oxygen dimol-sensitized luminescence, JACS, 1993, 115 (14), 6013-6016

[S3] Keller, K.; Mertens, V.; Qi, M.; Nalepa, A. I.; Godt, A.; Savitsky, A.; Jeschke, G.; Yulikov, M. Computing Distance Distributions from Dipolar Evolution Data with Overtones: RIDME Spectroscopy with Gd(Iii)-Based Spin Labels. Phys. Chem. Chem. Phys. 2017, 19 (27), 17856–17876.